CRYSTAL GROWTH UNDER BRIDGE FOUNDATIONS

A. Ramon (anna.ramon@upc.edu), E. Alonso
Department of Geotechnical Engineering and Geosciences.Universitat Politècnica de Catalunya, Barcelona, Spain.

ABSTRACT. A high-speed railway viaduct experienced a sustained heave at high rates after its construction. The pillars of the bridge are founded on an Eocene hard anhydritic-gypsiferous claystone by means of massive foundations. Field investigations identified an active layer below the piles' tips where expansions occur as a result of gypsum crystal growth in discontinuities from supersaturated aqueous solutions. The construction of the bridge is supposed to have triggered the swelling mechanism. An embankment, partially filling the valley, was built to slow the heave rate. The presence of soluble gypsum and anhydrite and inert materials is considered in the model developed to reproduce the observed expansive mechanism. The formulation describes the kinetics of dissolution and precipitation of minerals and the induced swelling strains by crystal growth. The calculated heave is compared with the field long-term vertical displacements measured before and after the construction of the embankment. A sensitivity study is also reported.

1. Heave of Pont de Candí viaduct

Pont de Candí viaduct belongs to the high-speed railway Madrid-Barcelona line in Spain. The construction of the bridge finished in July 2002. The viaduct is located between Camp Magré tunnel and Lilla tunnel, which experience also swelling damage. The bridge deck has a length of 413 m divided into 10 spans (35 m; 8 x 43 m and 34 m). The continuous deck has a box cross section with a thickness of 3.5 m. The deck is supported by 9 pillars (P1 to P9) with a maximum height of 56 m in the centre of the valley. Figure 1 shows a general view of the bridge in December 2007. Each pillar is founded by means of a massive foundation consisting of a group of 3 x 3 bored piles, 1.65 m in diameter and 20 m long on average, capped by a rigid slab as shown in Figure 2. The thickness of the pile cap in pillars P3 to P8 is 3.5 m.

Systematic levelling of the railway tracks, carried out by the railway administration since the end of the construction, revealed that the four central pillars of the bridge, especially pillars P5 and P6, were experiencing a sustained heave. The topographic levelling of the structure showed that in the period from September 2002 to May 2007 a maximum vertical displacement of 20 cm was reached at deck level between pillars P5 and P6. The heave measured at the structure evolved at high rates ranging from 5 to 10 mm/month.

The valley where Pont de Candí viaduct is placed is located in the eastern boundary of the Ebro river depression. The valley is the result of intense tectonic activity, which resulted in faults and folded strata. Sediments belong to old Tertiary formations. The valley is covered in its central part by a 5 meters thick deposit of soft alluvium and colluvium soils. These Quaternary deposits overly a 15 m thick layer of brown clays and gypsum levels of Eocene age. Below, there is a harder red claystone formation with variable contents of anhydrite and gypsum, also of Eocene age, which was judged strong enough to support the large diameter piles. A continuous horizontal gypsum layer (0.6-2 m thick) divides the red claystone unit into an upper and a lower level. The upper claystone level presents high gypsum content. Anhydrite was not detected in this upper level. In sharp contrast, the lower claystone unit below the thin continuous gypsum layer has high anhydrite content and an increased strength.

The sustained heave rates measured at the structure were incompatible with the expected circulation of trains at high speeds in excess of 300 km/h. A monitoring campaign of the structure and the subsoil was launched to understand the reasons of the vertical displacements observed in the bridge.

Figure 1. General view of Pont de Candí Bridge in Dec. 2007

2. Field investigations

Twelve boreholes with continuous recovery of cores where drilled along the axis of piles of the foundations of the four central pillars to study the state and the integrity of the foundations. The boreholes penetrated a few meters into the natural ground below the tip of the piles. No

cavities were found along the piles. The study of the walls of the boreholes revealed the existence of a fracture in the contact between the pile cap and the pile in almost all the piles investigated. The presence of the crack was interpreted initially to be the result of a shallow expanding layer located below the pile cap and exerting swelling pressures against pile caps while the pile shafts remained firmly anchored at depth in the hard claystone. An alternative and more consistent explanation is given in Sauter et al. (2012)

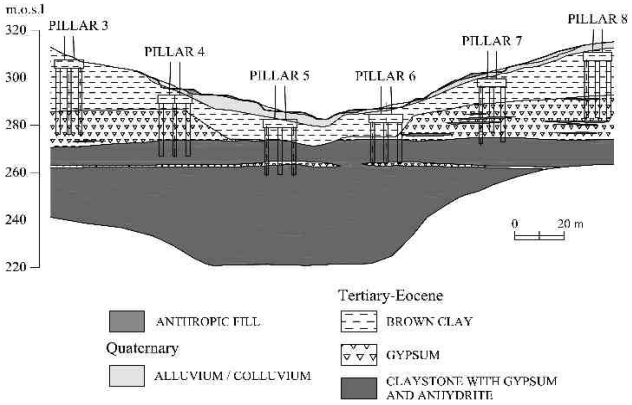

Figure 2. Geological profile along Pont de Candí viaduct.

The investigation of water levels, by means of open-tube piezometers, wells and excavated trenches in the bridge area indicated that a relatively shallow phreatic level, 5 m deep, exist at the lower part of the valley crossed by the bridge. A deep water level in the upper gypsiferous claystone was also identified.

Continuous and rod extensometers up to 60 m long were installed inside boreholes in the area between pillars P3 and P7 in order to study the behaviour of the subsoil in depth. Continuous extensometers recorded that increasing upward vertical strains were developing at depth in an active layer, 9-15 meters thick, located below the tip of the piles, under the gypsum level, within the anhydritic claystone. No significant movements were measured at shallower or deeper levels (Figure 3). The measurements of different extensometers allowed to estimate the position of the expanding active layer along the axis of the viaduct (Figure 4).

X-ray diffraction analyses were performed on samples recovered from different depths along the length of several extensometers. Profiles of anhydrite and gypsum content in depth were obtained. The comparison between the vertical distribution of anhydrite and gypsum contents with recorded swelling strains showed that swelling was directly associated with the presence of anhydrite. No swelling was recorded if only gypsum was present.

The expanding phenomenon resulted not only in the heave of piles and the viaduct itself, but also in a ground heave which could be measured by a network of surface topographic marks that covered an area 200 meters wide centred along the axis of the viaduct. In general the most significant heave were measured in an area around the central pillars of the bridge. In 5 months a maximum heave of 45 mm was measured in a topographic mark located 30 m away from the viaduct, near pillar P5. The evolution in time of the measured heave at the ground surface level followed a linear trend, and indicated that the heave phenomenon did not stabilize, and it even accelerated in some areas.

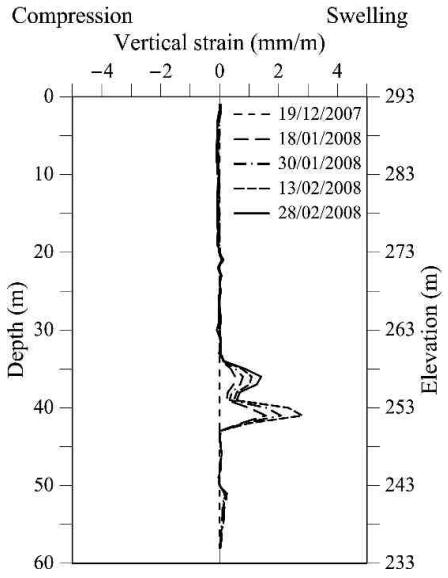

Figure 3. Vertical strains measured by sliding micrometerSL-1.

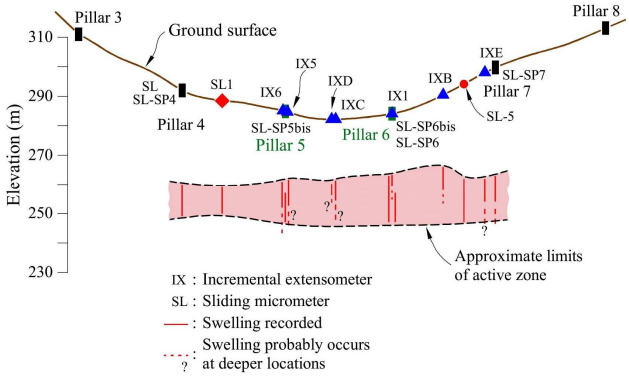

Figure 4. Longitudinal section along the viaduct between pillars P3 and P8. The location of the active expanding layer is shown.

The similarities between the vertical displacements measured on the viaduct and the heave measured at the ground surface along the axis of the bridge in the same period of time were in agreement with the fact that the heave of the bridge was due to the swelling layer located below the tip of the piles of the central pillars. A semi-analytic analysis verified that the cracks in the cap-pile contacts observed in borings performed through some piles were the result of the development of a non-homogeneous heave displacement of the piles belonging to a pile group (Sauter et al., 2012).

In order to investigate the structure, the existence of fractures and the connectivity of discontinuities in the active expanding layer, a hydraulic cross-hole campaign was performed. Four hydraulic cross-hole tests were performed on 3 boreholes, 50 m long, situated in an area with high heave located downstream of pillar 5. As a

reference, continuous extensometers in this area indicated the existence of an active layer, 14 m thick, which extends from elevations 246 to 260m. In order to perform one cross-hole test 3 stretches were isolated by means of two packers separated 7 m on each borehole. Four injection tests were performed by injecting a constant flow rate of water in the central section of one borehole. Packers were lowered in steps for each successive test in order to investigate the response of the claystone at different depths. During the injection tests, the water pressures were measured in time in the $3 \times 3 = 9$ stretches isolated in the three borings.

The analysis of the results of the cross-hole hydraulic tests showed that the active expanding layer had a system of open hydraulically connected horizontal discontinuities. No hydraulic connection could be established in a vertical direction. An average (horizontal) permeability of $2 \cdot 10^{-6}$m/s was calculated at elevations 265–243 m. Very low values of horizontal permeability were found above and below the active zone. The recovered cores from the boreholes presented an increased fracture density at depths of 22.5-35m. At higher depths the cores were massive.

3. The swelling phenomenon

The cores recovered from the boreholes performed for the installation of extensometers and for the cross-hole tests were studied in detail. Presence of gypsum crystal growth was observed on some open discontinuities in the material recovered from depths corresponding to the active expanding layer. Two different morphologies of gypsum crystals growth were found: gypsum crystal growth in needles was observed on open discontinuities, partially clogging the open fractures, oriented in a direction perpendicular to the plane of the discontinuity; and thin and warped sheets of gypsum embedded in the rock matrix (Figure 5).

These field observations indicated that the swelling detected in the active expanding layer could be related with gypsum crystal growth and that the presence of anhydrite plays an important role in the expanding mechanism.

a) *b)*

Figure 5. Gypsum crystal growth in recovered cores from boreholes at depths corresponding to the active layer a) needles filling partially a discontinuity, b) laminar gypsum crystal growth developing inside the clay matrix

Gypsum crystals precipitate from supersaturated water in calcium sulphate. The experimental work of Kontrec et al. (2002) describes the spontaneous precipitation of gypsum from the supersaturated solutions in equilibrium with anhydrite crystals in suspension in the solution. There is no need for a pre-existing gypsum crystal for further gypsum crystal growth, although the presence of gypsum crystals facilitates gypsum precipitation. Figure 6 provides the variation of anhydrite and gypsum solubilities in pure water with temperature. Since the solubility of anhydrite ($CaSO_4$) is higher than the solubility of gypsum ($CaSO_4 \cdot H_2O$) below 56ºC, water in contact with the anhydritic claystone will tend to dissolve anhydrite, supersaturation conditions with respect to gypsum will be reached and the excess of dissolved calcium sulphate ($CaSO_4$) will tend to precipitate in gypsum crystals. This mechanism may lead, in time, to the transformation of all available anhydrite into gypsum if water in contact with anhydrite mineral exists.

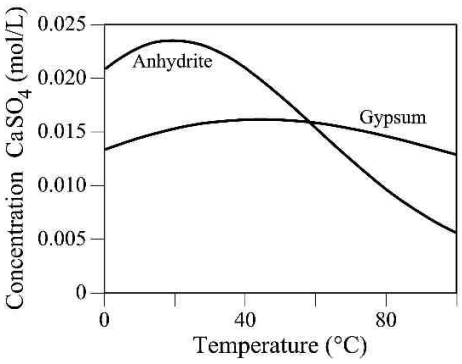

Figure 6. Equilibrium concentration of $CaSO_4$ in calcium sulphated water with respect to anhydrite and gypsum.

The swelling phenomena present in Pont de Candí has been also observed under the invert of Lilla tunnel, excavated near Pont de Candí bridge in an Eocene sulphated claystone formation (Alonso et al. 2012), and also in other tunnels excavated in Triassic claystone formations containing sulphate species in Central Europe. Experience in tunnels indicate that the active expanding zone is located under the tunnel floor, where the highest stress release is experienced and therefore the highest risk of opening new or existing discontinuities occurs.

Precipitation of crystals occurs more easily if some “open” space is available. Pores of claystones provide an extremely reduced space and water flow is essentially restrained through them. But joints provide a more favourable environment for crystal growth: the “open” space increases dramatically, as well as the permeability. A conceptual representation of this interpretation is illustrated in Figure 7. Swelling will be controlled not only by the total mass of the precipitated gypsum (which may occur at a distance from the source of anhydrite dissolution) but also by the geometry of precipitated crystals and its interaction with the surrounding soil/rock.

The hydraulic cross-hole tests performed revealed the existence of horizontal hydraulically connected fractures in the active layer which provided the necessary open space for gypsum crystals to grow and also confirmed the presence of circulating water. The process of precipitation of gypsum in discontinuities is thought to act as a local

jacking effect pushing apart the rock mass, capable of opening discontinuities and inducing swelling strains.

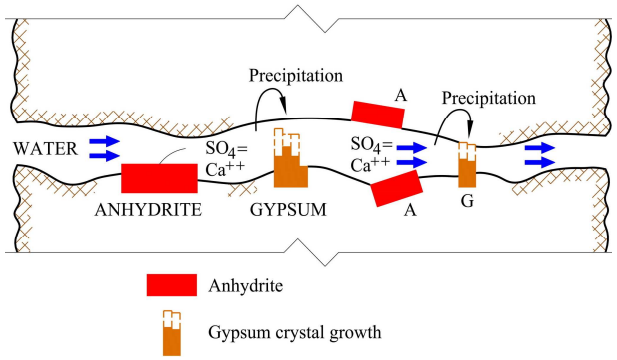

Figure 7. Conceptual model for gypsum precipitation.

The development of the swelling phenomena in depth is thought to be associated with the construction of the bridge. The boreholes drilled at the beginning of the design stage and the construction of the piles connected the upper aquifer with the deep fractured claystone. The water entrance into the horizontal open fractures triggered the swelling phenomena.

4. Remedial measures

An embankment 33 m high over the lowest elevation of the valley was built partially filling the valley of Pont de Candí viaduct from October 2009 to August 2010. This remedial measure was inspired by the belief that applying vertical stress on the active layer would reduce the rate of heave and eventually would be able to eliminate it. The rate of measured heave on the structure after the construction of the embankment decreased. Sliding micrometers measured a decreasing rate of vertical strains in the active layer after the construction of the embankment. Compressive strains were also measured in the layers above the active layer some time after the application of embankment loading (Figure 8).

5. Model formulation

The swelling phenomenon has been formulated within a general framework of hydro-mechanical analysis for saturated and unsaturated porous media. The material involved in the swelling mechanism is not a standard material. The formulation of the specific problem of swelling due to gypsum crystal growth has to take into account the presence of gypsum and anhydrite, which are soluble minerals, apart from the insoluble clay minerals. The model needs to follow the transport of solute. Also the processes of dissolution and precipitation of sulphate minerals and its mechanical and hydraulic effects have to be described by the formulation.

A porosity is defined for anhydrite and gypsum crystals, ϕ_{anh} and ϕ_{gyp}, which describe the fraction of total volume occupied by crystals. The mass balance of solid phase now requires three balance equations, one for each solid species (the insoluble solids and the soluble gypsum and anhydrite minerals):

$$\frac{\partial}{\partial t}\left(\rho_s\left(1-\phi-\phi_{anh}-\phi_{gyp}\right)\right)+ \\ +\nabla\cdot\left[\left(\rho_s\left(1-\phi-\phi_{anh}-\phi_{gyp}\right)\right)\frac{d\boldsymbol{u}}{dt}\right]=0 \quad (1)$$

$$\frac{\partial\left(\rho_{gyp}\phi_{gyp}\right)}{\partial t}+\nabla\cdot\left[\left(\rho_{gyp}\phi_{gyp}\right)\frac{d\boldsymbol{u}}{dt}\right]=\frac{dm_{gyp}}{dt} \quad (2)$$

$$\frac{\partial\left(\rho_{anh}\phi_{anh}\right)}{\partial t}+\nabla\cdot\left[\left(\rho_{anh}\phi_{anh}\right)\frac{d\boldsymbol{u}}{dt}\right]=\frac{dm_{anh}}{dt} \quad (3)$$

The first equation describes the mass balance of the insoluble clay. It is the classical equation for mass balance of solid phase in standard soils. ρ_s, ρ_{gyp} and ρ_{anh} are the densities of the insoluble minerals, gypsum and anhydrite, and $\boldsymbol{u}$ is the displacement vector, which is accepted as a unique field for the porous medium. The rates of precipitated or dissolved mass of gypsum and anhydrite (dm/dt) are introduced in the mass balances of the soluble solid phases (gypsum and anhydrite) described in Eq. 2 and Eq. 3. Combining the three equations and accepting that the densities ρ_s, ρ_{gyp} and ρ_{anh} are constant, the variation of porosity in time becomes,

$$\frac{D_s\phi}{Dt}=\left(1-\phi\right)\nabla\cdot\left(\frac{d\boldsymbol{u}}{dt}\right)-\frac{1}{\rho_{gyp}}\frac{dm_{gyp}}{dt}-\frac{1}{\rho_{anh}}\frac{dm_{anh}}{dt} \quad (4)$$

where $\frac{D_s(\bullet)}{Dt}=\frac{\partial(\bullet)}{\partial t}+\frac{d\boldsymbol{u}}{dt}\cdot\nabla(\bullet)$ is the material derivative.

Eq. 4 indicates that the variation in porosity in time has two components, the volumetric strain rate induced by solid displacements and the volumetric strain rate induced by the precipitation or dissolution of crystals.

The kinetics of precipitation/dissolution of gypsum and anhydrite are described by means of two mass rate equations with the same structure, one for each mineral. In the case of gypsum kinetics:

$$\frac{dm_{gyp}}{dt}=\sigma_c\kappa\xi_{gyp}\phi_{gyp}\left(\left|\left(\frac{\omega_l^m}{\omega_{l_{sat,gyp}}^m\left(T,p\right)}\right)^{\theta}-1\right|\right)^{\eta} \quad (5)$$

$$\text{where } \xi_{gyp}=\frac{\omega_l^m-\omega_{l_{sat,gyp}}^m}{\left|\omega_l^m-\omega_{l_{sat,gyp}}^m\right|} \quad (6)$$

where, ω_l^m is the mass fraction of dissolved sulphate in water. The precipitated or dissolved mass of mineral in time depends on: the "degree" of superasaturation or undersaturation, the volumetric fraction of mineral crystals, ϕ_{anh} and ϕ_{gyp}, the specific surface of crystals, σ_c (m^2 of crystal surface/m^3 of crystal) and a rate constant κ ($kg/(s\cdot m^2)$). The equilibrium mass fraction of calcium sulphate in water at saturation conditions with respect to gypsum ($\omega_{l_{sat,gyp}}^m$) and with respect to anhydrite are

considered dependent on temperature, *T*, and on the prevailing pressure acting on crystals, *p*, as described by Scherer (1999):

$$\omega_{l_{sat}}^{m} = \omega_{0l_{sat}}^{m} \exp\left(\frac{p v_c}{R_g T}\right) \qquad (7)$$

where, v_c is the molar volume of the crystal; R_g is the ideal gas constant, and T is the absolute temperature. Temperature was constant in the case analyzed. This was probably the situation in the active region below the pile's tip.

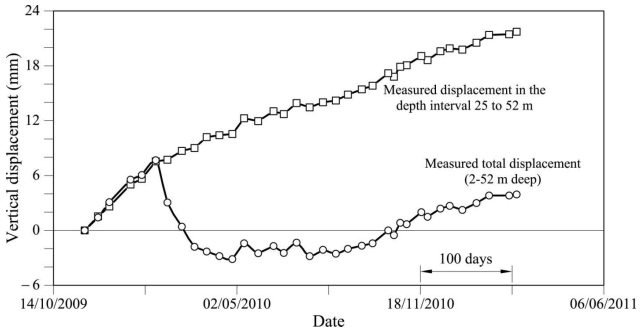

Figure 8. Evolution of the integral values of vertical strains measured between pillars P6 and P7 by an sliding micrometer.

Gypsum precipitation incorporates molecules of water in its crystalline structure. This process is taken into account in the source/sink term of the mass balance of water equation.

The mechanical effects of gypsum crystals precipitation are taken into account in the momentum balance of the medium. The strains induced by precipitation of gypsum are calculated from the amount of precipitated volume of gypsum and the prevailing stress acting on crystals.

$$\frac{d\varepsilon_i}{dt} = \frac{\gamma_i}{\rho_{gyp}} \frac{dm_{gyp}}{dt} \quad , \quad i = 1,\ 2,\ 3 \ ; \qquad (8)$$

1=Vertical (z) ; 2, 3= Horizontal (h)

The parameter γ_i is a coefficient that takes into account the effect of the stress applied on crystals on the strains induced by precipitation.

$$\gamma_i = \gamma_{max} e^{-b\sigma_i'} \text{ for } \sigma_i' > 0,\ i=1,\ 2,\ 3 \qquad (9a)$$

$$\gamma_i = \gamma_{max} \text{ for } \sigma_i' = 0,\ i=1,\ 2,\ 3 \qquad (9b)$$

A given volume of precipitated crystals is expected to induce higher swelling strains under a lower confining stress.

The model needs to keep track of the minerals dissolved in water. Dissolution of anhydrite and gypsum results in calcium sulphate solute ($CaSO_4$). Then, one equation for the mass conservation of solute is formulated for calcium sulphate solute transport:

$$\rho_l \omega_l^m \nabla \cdot \left(\frac{du}{dt}\right) + \phi \frac{D_s\left(\rho_l \omega_l^m\right)}{Dt} + \nabla \cdot \left(\rho_l \omega_l^m q_l - \boldsymbol{D} \nabla \cdot \omega_l^m\right) =$$
$$= -\frac{dm_{gyp}}{dt}\left(1 - \frac{\rho_l \omega_l^m}{\rho_{gyp}}\right) - \frac{dm_{anh}}{dt}\left(1 - \frac{\rho_l \omega_l^m}{\rho_{anh}}\right) \qquad (10)$$

In this equation the product $\rho_l \omega_l^m$ is the concentration of sulphate in water in units of mass/volume. The term $\boldsymbol{D} \nabla \cdot \omega_l^m$ accounts for the diffusive rate of flow following a Fick's law. $\boldsymbol{D}$ is the diffusion coefficient. The precipitation and dissolution of sulphated minerals are treated as a source or sink of calcium sulphate solute.

This formulation was included in the Finite Element program for coupled thermo-hydro-mechanical analysis in porous media CODE BRIGHT (DETCG, 2010 and DIT-UPC 2002)

6. Simulation of Pont de Candí expanding mechanism

A column 15 m wide and 55 m long of the foundation material at the central pillar of the bridge (P5) has been modelled under plane strain conditions. Figure 9 shows the geometry of the model. The active layer, 15 m thick, was included at the position estimated by the sliding micrometers. Below and above the active layer the soil is non expansive. The column of foundation material was assumed to be confined laterally. An inert material was used at both sides of the column to facilitate the definition of the flow boundary conditions. The horizontal flow conditions in the active layer were reproduced. A phreatic level was defined above the active layer and a horizontal flux of water was imposed in the active zone. The fractured and highly permeable sulphated claystone was modelled as a porous material with high porosity (0.09).

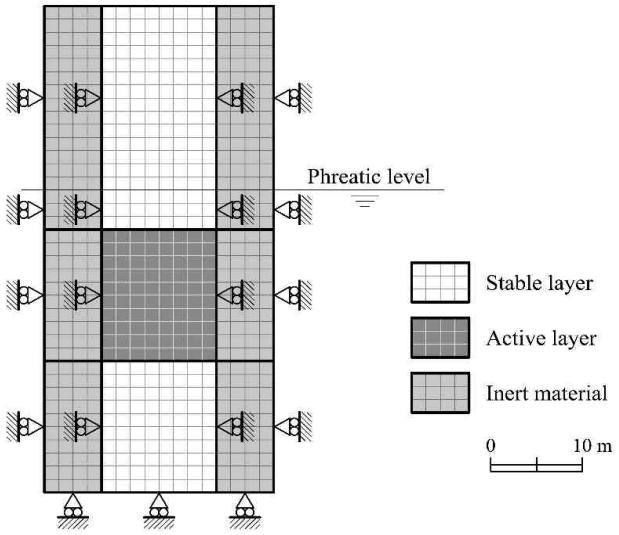

Figure 9. Finite element model geometry.

The initial mineral porosities were approximated from observations in recovered cores. The compound kinetic coefficient, $\sigma_c \cdot \kappa$, was back calculated by matching the swelling records with the calculated heave. The hydraulic

characteristics of the material were defined by the initial open porosity and the intrinsic permeability. The initial open porosity (0.09) was higher than conventional porosity to account for fissures. The permeability of $2 \cdot 10^{13}$ m^2 found in the cross-hole hydraulic tests was adopted for the intrinsic permeability in the active layer. An isotropic linear elastic behaviour was considered for the material of the column. The initial state of stress was given by an at rest earth pressure coefficient K_0=2.

The comparison between the calculated heave at the surface of the column and the evolution of the heave measured by topographic levelling at the ground surface level is represented in Figure 10. The vertical strains due to crystal growth only occur in the active layer and the material located above the active layer is pushed upwards.

The calculated vertical displacements reproduced the field heave records in the four years period modelled. The construction of the embankment was simulated with by applying a loading at the upper boundary of the column. The model reacts to embankment construction and the calculated vertical displacement reproduces the field measurements recorded after the "construction" of the embankment (t=924 days in Figure 10).

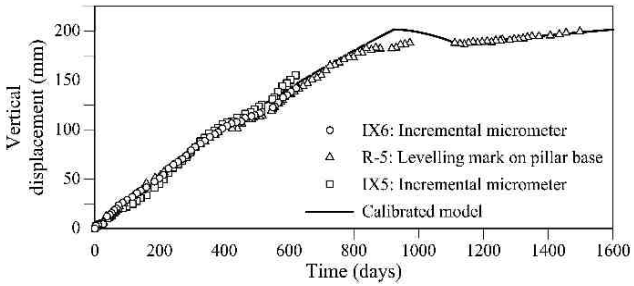

Figure 10. Measured and calculated surface heave.

A sensitivity analysis was performed to study the relevance of the model parameters. The model described was considered as a base case. For the study of the effect of each parameter only the value of the parameter analyzed was changed, and the other parameters maintained the value they had in the base case. It was found that the initial mineral content has an important effect on the development of heave because it controls the rates of dissolution and precipitation (Eq. 5). Gypsum content has a small effect. However, anhydrite volumetric fraction has a very significant effect on calculated swelling. The value of equilibrium concentration at saturation with respect to gypsum and anhydrite, which depends on temperature, has also a significant effect on vertical strains. Stress effects are substantial in the model developed. In contrast, the initial porosity, the permeability and the induced gradient have minor effect on the calculated heave.

7. Conclusions

The case of the heave of Pont de Candí viaduct has been described. Field investigations carried out in the valley demonstrated that the existence of an expanding layer located below the tips of the piles originated the sustained heave of the structure and also of the ground surface.

The swelling process is related with gypsum crystallization in fissures. The crystallization of gypsum in discontinuities produces a jacking effect pushing upwards the soil and rock layers above the active zone, as well as the bridge pillars. The hydraulic connection in the active expanding layer, revealed by hydraulic cross-hole tests, explains the presence of water and the existence of fractures, necessary for gypsum crystal growth. It is believed that the set of boreholes and foundation piles connected the upper aquifer with the deeper fissured anhydritic claystone, triggering the swelling phenomenon. Heave rate was reduced to a small value by the weight added by an embankment 33 m high which partially fills the original valley.

A model was developed for simulating the expansion in sulphated rocks due to gypsum crystal growth. The presence of soluble sulphated minerals and the occurrence of precipitation and dissolution of crystals have been considered in the formulations. The sensitivity analysis performed indicated that the initial anhydrite and gypsum content, the concentration of sulphate in equilibrium with respect to gypsum and anhydrite and, especially, the confining stress have a relevant effect on the swelling strains calculated in the model developed. A simulation of the conditions in the foundation material of Pont de Candí has been performed. Measured heave is reproduced by the model. The tool developed is believed to constitute a step forward in the analysis and prediction of swelling phenomena in sulphate bearing clay rocks.

8. Aknowledgements

The authors acknowledge with thanks the support provided by ADIF (National Agency for Railway Infrastructure). Thanks are also given to contractors FCC and IIC, for their helpful discussions and their contribution to the identification and characterization of the geotechnical conditions of the foundations, and to professors of the Department of Crystallography of the University of Barcelona for the conceptual discussions on the conditions of crystal growth.

9. References

Alonso, E.E., Berdugo, I.R. and Ramon, A. (2012). Extreme expansive phenomena in anhydritic-gypsiferous claystones: the case of Lilla tunnel. *Géotechnique*, in print.

DETCG (2010). CODE_BRIGHT User's Guide. Available on-line: https://www.etcg.upc.edu/recerca/code_bright.

DIT-UPC (2002). *CODE_BRIGHT, a 3-D program for thermo-hydro-mechanical analysis in geological media: User's guide*, CIMNE, Barcelona.

Kontrec, J., Kralj, D. & Brečević, L. (2002). Transformation of anhydrous calcium sulphate into calcium sulphate dihydrate in aqueous solutions. *J. Crystal Growth*, 240, 203-211.

Scherer, G. (1999). Crystallization in pores. *Cement and Concrete Research*, 29, 1347-1358.

Sauter, S., Alonso, E.E. and Ramon, A. (2012). Efecto de la expansión profunda sobre cimentaciones por pilotes. *Proceedings of the SEMR and SEMSIG 9th National Symposium*, Sevilla, 385-397.